超轻质磁性石墨烯/炭气凝胶的制备及电磁干扰性能

张恩爽， 雷朝帅， 李 健， 刘圆圆， 高宇智， 吕 通， 李文静， 张 昊
（航天特种材料及工艺技术研究所，北京 100074）

摘 要： 通过溶胶-凝胶、超临界干燥及高温裂解过程制备了 Fe_3O_4 磁性纳米粒子掺杂的石墨烯/炭气凝胶，该气凝胶具有多组分、超轻质及高导电等特性。研究了不同 Fe_3O_4 磁性纳米粒子掺杂量对材料微观结构、组分及电磁干扰性能的影响规律，获得密度仅为 0.015 g cm^{-5}，比表面积为 511 m^2 g^{-1} 的分等级微纳米结构的超混杂气凝胶材料。该材料可以实现对3种波段的有效遮蔽，对可见光在布撒初期和30 min后遮蔽率分别是99.90%和98.77%，对于3～5 μm红外及8～12 μm红外布撒初期的遮蔽率分别是99.55%和99.35%，布撒30 min后遮蔽率分别是99.05%和96.79%，对毫米波的干扰性能在布撒初期和30 min后遮蔽率分别是83.68%和82.54%。该材料优异的多波段电磁干扰性能为高性能烟幕干扰材料提供了新的设计思路。

关键词： 轻质；磁性；气凝胶；电磁干扰；烟幕
中图分类号： O69 **文献标识码：** A

基金项目：国家自然科学基金（51803203）.
通讯作者：李文静，教授. E-mail：ht3lwj@126.com
张 昊，教授. E-mail：ruizhangh@163.com
作者简介：张恩爽. E-mail：zhanges@126.com

The preparation of super lightweight magnetic Fe_3O_4/graphene/carbon aerogels and their use in electromagnetic interference shielding

ZHANG En-shuang， LEI Chao-shuai， LI Jian， LIU Yuan-yuan，
GAO Yu-zhi， LU Tong， LI Wen-jing， ZHANG Hao
（*Aerospace Institute of Advanced Material& Processing Technology*, *Beijing* 100074, *China*）

Abstract： Magnetic Fe_3O_4/graphene/carbon aerogels were prepared by the sol-gel method, followed by supercritical drying and pyrolysis. The microstructures, electrical properties and electromagnetic interference shielding performance of the aerogels were investigated. The aerogels were crushed into a fine powder with a bimodal particle size distribution (～0.1 and 10 μm) and released into a chamber to a particle concentration of 1 g m^{-3} at room temperature under atmosphere pressure using a dispensing device, where electromagnetic interference shielding was tested. Results indicate that the composite aerogels have high conductivity and a hierarchical pore structure with a density as low as 0.015 g cm^{-3}. The concentration of the fine powder in the chamber decreased with time and levelled off above 20 min. The shielding is dominated by the particles that are difficult to settle due to their perturbation by air. The shielding for the visible wave band of the composite aerogels in powder form initially and after the release for 30 min are above 99.90% and 98.77%, respectively. Those for 3-5 μm and 8－12 μm infrared light are respectively 99.55% and 99.35% initially, and 99.05% and 96.79% after the release for 30 min. For the millimeter wave band, the shielding ratios initially and after the release for 30 min are above 83.68% and 82.54%, respectively.
Key words： Lightweight; Magnetic; Aerogel; Electromagnetic interference; Smoke screen

Received date: 2019-08-23; *Revised date*: 2020-09-22
Foundation item: National Natural Science Foundation of China (51803203).
Corresponding author: LI Wen-jing, Professor. E-mail: ht3lwj@126.com
ZHANG Hao, Professor. E-mail: ruizhangh@163.com
Author introduction: ZHANG En-shuang. E-mail: zhanges@126.com

1 Introduction

Smokescreen interference is one of the most widely used photoelectric passive interference method, which is achieved by releasing a great deal of aerosols. The aerosol particles that could change the

transmission path of light radiation to avoid objective have been discovered[1]. As the smokescreen interference materials have grown more diverse, smokescreen interference has been used as an effective means of optoelectronic countermeasures. Therefore, this has become an important field of concern for researchers[2-8]. However, the increasingly complex optoelectronic countermeasures have higher requirements for materials, such as low density, multi-frequency shielding and efficient shielding. Most of the existing smokescreen materials are expanded graphite, conductive fiber, metal nanometer powder and their mixtures. In the application of these traditional materials, there are many problems such as single shielding band, high density and complex distribution [9-11].

In order to solve these problems, the researchers developed new material systems to improve the performance of traditional materials. Yu et al[12] prepared the MMW/IR composite interference material from carbon fiber, copper-coated carbon fiber, conductive carbon powder and other components. The material shows an attenuation of 12.7-16.4 dB and 21.2-33.3 dB for 3 mm and 8 mm waves (MMW), respectively. However, the infrared light (IR) also has 85%-90% of the shielding. To realize two bands of effective shielding, Liu et al[13] studied the smoke interference performance of short cut carbon fibers, which had excellent dual band interference performance for MMW/IR. The maximum attenuation ratio at the band range of 3 mm and 8 mm waves was above 95%, and the effective time could be greater than 30 s, and the maximum attenuation ratio was close to 100% for 8-14 μm IR, but its effective time was only 20 s[13]. Chen et al explored the interference properties of carbon nanotubes/graphene/carbon composites as the infrared smoke. The result showed that the shading ratio of middle infrared band (3-5 μm) was above 95%, and the effective time was 372 s. For the far-infrared (8-14 μm), the shading ratio was up to 96%, and the effective time was 441 s[14].

For the effective and practical smokescreen interference material systems, being lightweight is an important technological requirement. In our recent report, we creatively fabricated a unique conductive graphene-doped carbon aerogel powder and preliminarily demonstrated its potential application for electromagnetic interference in the frequency range of visible light (94%), infrared (97%) light and millimeter wave (75%), effective time could be greater than 10 min[15].

In summary, the above-mentioned researches fully demonstrate that, it is difficult for the existing material systems to simultaneously meet the requirements of multi-band and long time electromagnetic interference applications [16,17]. The electromagnetic interference effect of smokescreen materials depends on many factors, including the conductivity, microstructure, particle size and density. For the smokescreen interference material, a multi-band smokescreen for infrared/visible/millimeter wave must have an important feature of a wide particle size distribution. Especially, the particle size of the millimeter wave smoke must be on the order of millimeters. How to avoid the rapid settlement of large particles due to gravity is an important issue to be solved.

Aerogels are low density nano-porous non-crystalline solids whose structures can be controlled through preparation [18-20]. Here we demonstrate design and fabrication of an ultra-lightweight and highly conductive graphene/carbon/Fe_3O_4 aerogel powder for high-performance electromagnetic interference application. The graphene/carbon/Fe_3O_4 (GN/CA/Fe_3O_4) aerogel powder formed by this method shows a density as low as ~0.023 g cm^{-3}, about 30 times smaller than that of a common metal powder. It's worth noting that shielding ratio of the composite aerogel powder is above 99.90% and 98.77% in visible wave band, respectively, at the beginning of release and after 30 min. At the beginning of release, the shielding ratio is 99.55% and 99.35% in 3-5 μm and 8-12 μm infrared light, respectively, it is 99.05% and 96.79% after 30 min. For millimeter wave band, the shielding ratio of the composite aerogel powder is above 83.68% and 82.54%, at the beginning of release and after 30 min, respectively. The study is expected to extend the application of smoke jamming[21,22].

2 Materials and methods

2.1 Chemical materials

Unless otherwise specified, all other reagents were of analytical grade and used as received without further purification, and all solutions were prepared with distilled water. Sodium carbonate anhydrous (Na_2CO_3, 99.5%, Tianjin Fuchen), ethanol (anhydrous, 99.8%, Aladdin), formaldehyde solution (analytical standard, 0.748 mg L^{-1} in water), resorcinol (98%, InnoCHEM), graphene oxide gel (20 g L^{-1}, Xinyihua).

2.2 Preparation of the graphene/carbon / Fe_3O_4 aerogel powders

The graphene/carbon/Fe_3O_4 aerogels were prepared through the following procedure. Resorcinol and formaldehyde with a 1∶2 molar ratio were mixed with sodium carbonate and water at a mass ratio of

1∶1000. The solution was magnetically stirred for ~0.5 h in a capped bottle at room temperature. Subsequently, the graphene oxide solution (0-25 mL) is added to the above solution(100 mL). The above solution was magnetically stirred for 0.5 h in a capped.

The mixture was injected into a mold of a certain size, then placed in the oven, and kept for 72 h at 80 °C. Then the gel monoliths were soaked in a bath of $FeCl_3$ solution ($0^{\#}$:0.00 g mL^{-1}, $1^{\#}$:0.05 g mL^{-1}, $2^{\#}$:0.10 g mL^{-1}, $3^{\#}$:0.20 g mL^{-1}) for three days (25 °C). The gels were removed from $FeCl_3$ solution and soaked in ethanol for 72 h. Repeating this step for three times, the Fe^{3+}-modified phenolic aldehyde aerogel composites were obtained by supercritical drying.

The Fe^{3+}-modified phenolic aldehyde aerogels were carbonized at a heating rate of 5 °C min^{-1} to 1 000 °C and then held for 4 h in N_2 to obtain the graphene/carbon/Fe_3O_4 aerogel composites. Finally, the aerogel was mechanically crushed to form aerogel powder. The preparation steps for the modified Fe_4O_3/GN/CA is schematically represented in Fig. 1.

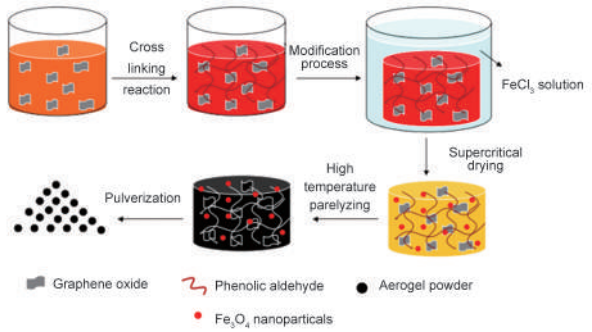

Fig. 1　Schematic illustration of fabrication process for the magnetic graphene/carbon/Fe_3O_4 aerogel powder.

2.3　Characterization of electromagnetic properties of the composite aerogel powder

The electromagnetic properties of the aerogel powder were measured in a test system consisting of a transmitter, a smoke chamber and a receiving device. The smoke chamber was made of polythene plastic sheets (6.1 m×2.0 m×6.8 m). To test electromagnetic interference properties, aerogel powder (1 g m^{-3}) was released into the smoke chamber through a dispenses device. After scattering, the optical path passed through the aerogel powder, transmittance or attenuation data were collected by the receiver. At the same time, the floating aerogel powder was extracted at different time points to test its concentration, and the variation of stagnated air powder concentration with time was obtained.

2.4　Instrumentation and characterization

The weight of the aerogel powder was measured by an electronic balance with an accuracy of 0.01 mg. The morphology on the aerogels was obtained by a SEM (HITACHI, SU8000) and TEM (FEI, F30). The dimensions of macroscopic specimens were determined via a vernier caliper with an accuracy of 0.02 mm. The Particle size distribution was obtained on a mastersizer (UK, Malvern 2000). The crystalline structure was identified by using X-ray diffraction (XRD, D/max-2500, Rigaku) with Cu Ka radiation at a scanning rate of 0.5 and 7° min^{-1} with 2θ ranging from 20° to 80°. The specific surface area and pore volume were measured by Brunauer-Emmett-Teller (BET) and Barrett-Joyner-Halenda (BJH) methods using an NOVA 2200e surface area analyzer (Quantachrome). The Electromagnetic interference properties were tested by SR-5000N infrared spectrum radiometer, millimeter wave test system (3 mm) and visible visibility meter (CN, Chengdu University of Electronic Science And Technology).

3　Results and discussion

3.1　Chemical composition and micro-structure

Fig. 2 shows the typical scanning electron microscopy (SEM) images of aerogel powders with different doping amounts of magnetic particles. $0^{\#}$ is the sample before doping, $1^{\#}$-$3^{\#}$ are aerogel powders with different magnetic particle doping concentrations. One can observe that $0^{\#}$-$3^{\#}$ aerogel powders exhibit hierarchical micro-nanostructures. The hierarchical structure is composed of micron-scale graphene sheets and nanoparticles distributed between them. With the change of the doping concentration, the hierarchical structure has no obvious change. Graphene sheets are micron-sized monolayer. The interlamellar nanoparticles (10-20 nm) are evenly distributed between the lamellae and form a composite structure.

As Fe^{3+} reacts with the functional groups on the surface of GO and hydroxyl groups in phenolic aldehyde during impregnation, Fe^{3+} forms Fe-based coupling materials, and magnetic nanoparticles are formed during the supercritical drying and pyrolysis. In order to observe the existence form of Fe element in the doped aerogels, EDS test was carried out for $1^{\#}$-$3^{\#}$ samples, and the results are shown in Table 1. The main contents of the $0^{\#}$-$3^{\#}$ samples are carbon from phenolic and GO pyrolysis (over 60%), followed by O from partial phenolic and GO pyrolysis incompletely or newly formed oxides (10%-30%), and Fe from doping (3%-11%). It can be seen from the energy spectrum of Fe element (Fig. 3) that with

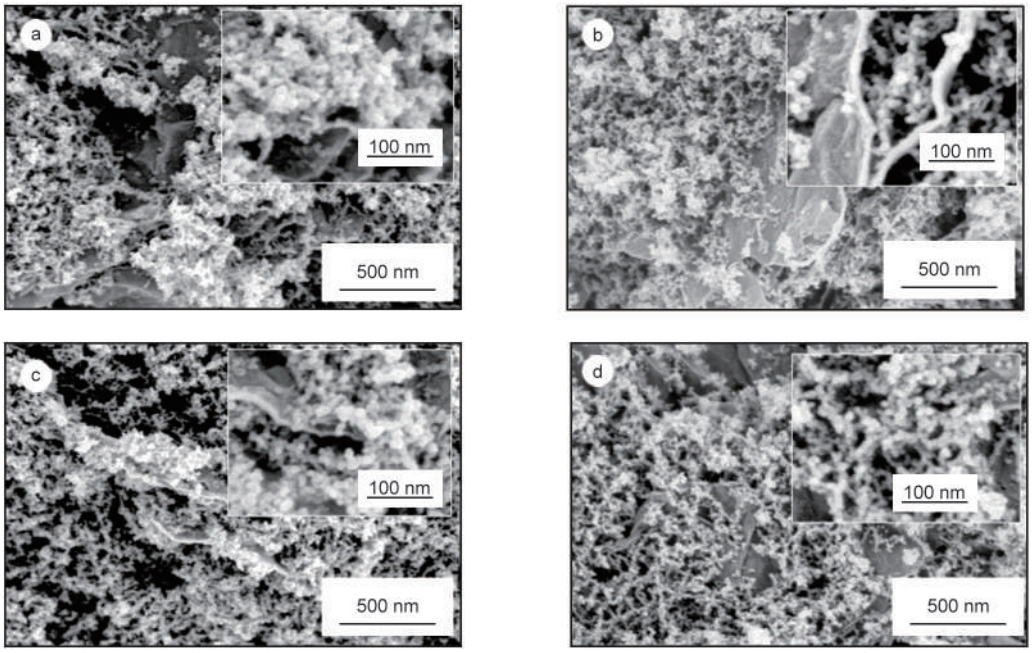

Fig. 2 SEM images of the aerogel powders: (a) 0#, (b) 1#, (c) 2# and (d) 3#.

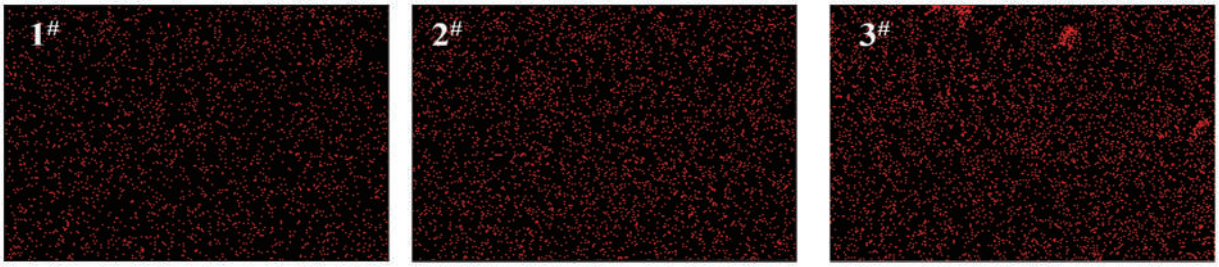

Fig. 3 EDS images and Fe element distribution of aerogels.

the increase of the doping concentration, the content of Fe on the surface of the material increases gradually. This indicates that with the increase of the concentration of Fe^{3+} in the solution, the adsorption of phenolic wet gel for Fe^{3+} increases, leading to the increase of Fe-compound content in the final system.

Table 1 Related element distribution of aerogels.

No.	O(%)	C(%)	Fe(%)
0#	11.40	88.60	0.00
1#	25.62	70.62	3.76
2#	26.62	66.76	6.62
3#	27.11	61.10	11.79

Fig. 5 shows the nitrogen absorption and desorption curves of the aerogels before and after doping. According to the distribution characteristics of the curves in the Fig. 5, it is found that $0^{\#}$-$3^{\#}$ all show a typical type IV adsorption-desorption isotherms, typical of mesoporous adsorption. In addition, in the range of p/p_0 = 0.7-1.0, there are obvious hysteresis loops, which indicates that the material has obvious capillary condensation and multi-layer adsorption phenomenon in nitrogen adsorption. The adsorption-desorption curves show that the aerogel hysteresis loop does not change significantly with the increase of Fe^{3+} doping. According to the data in Table 2, the specific surface areas of $0^{\#}$, $1^{\#}$, $2^{\#}$ and $3^{\#}$ samples are 495, 511, 528 and 548 $m^2\ g^{-1}$, respectively. This indicates that the addition of Fe^{3+} does not significantly change the pore structure of the material, and the slight increase of specific surface area may be caused by the increase of nanoparticles in the material due to doping.

At the same time, the average pore sizes of the measured nanometer holes are 23.5, 16.5, 16.1 and 14.5 nm for $0^{\#}$, $1^{\#}$, $2^{\#}$ and $3^{\#}$ samples, respectively. The decrease of pore size may be caused by the filling of the nanometer pores by doped iron nanoparticles. In addition, it can be seen from the Table 2 that the conductivity of the doped material decreases, which may be due to the presence of Fe-compounds in the form of oxides, which have a low conductivity. So

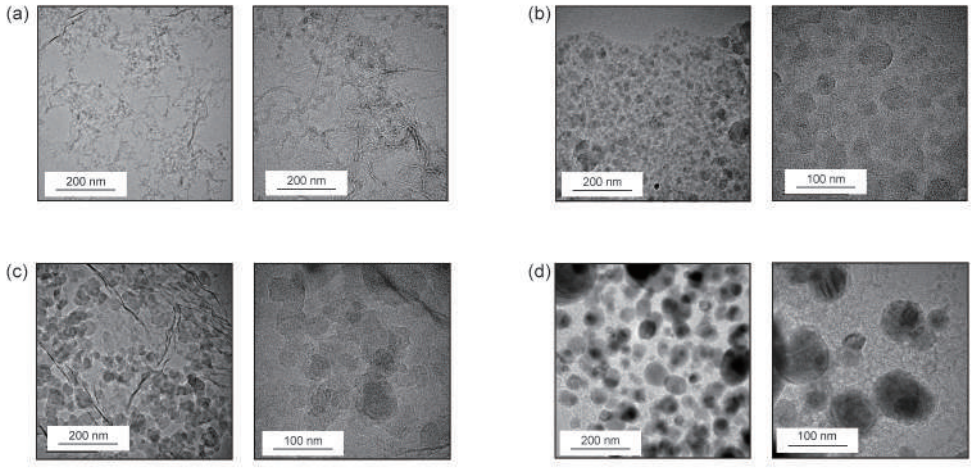

Fig. 4　TEM images of the aerogel powder: (a) 0#, (b)1#, (c)2# and (d) 3#.

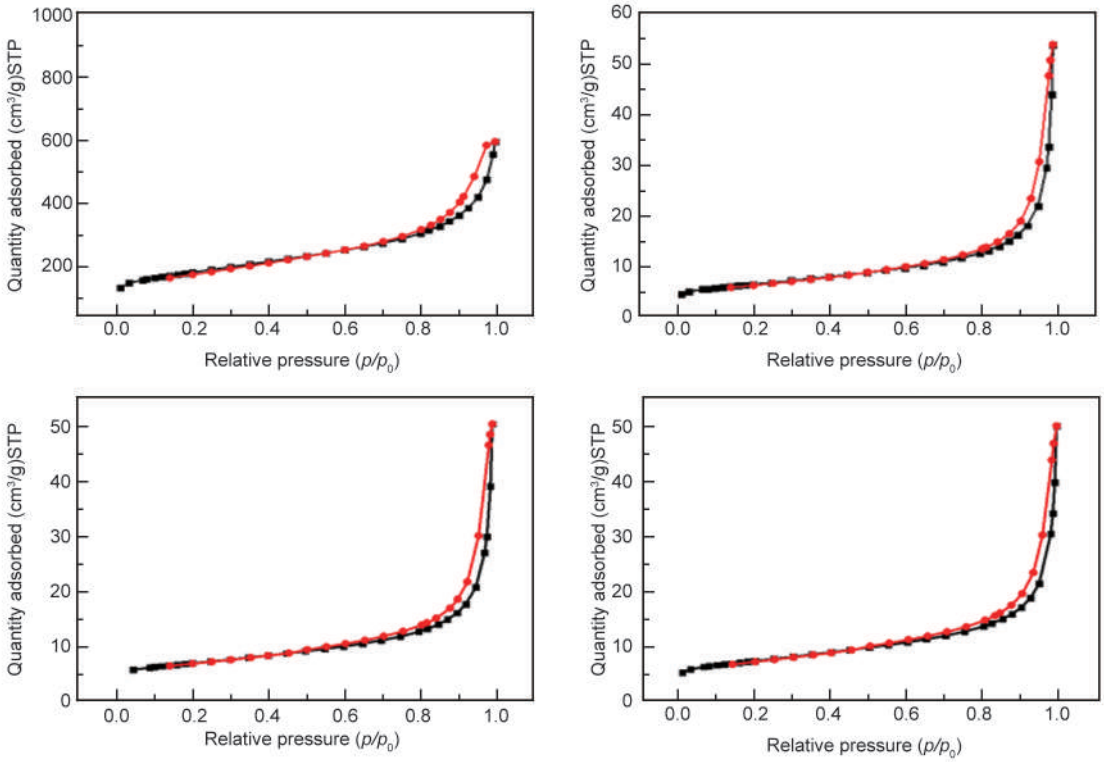

Fig. 5　Nitrogen sorption isotherms of the aerogel powders: (a) 0#, (b)1#, (c)2# and (d) 3#.

the presence of the iron-based nanoparticles slightly reduces the conductivity of the material, but has less impact on the material's conductivity

Table 2　Performance comparison of aerogel powders with various doping levels of Fe_3O_4.

No.	Density (g/cm^3)	BET (m^2/g)	Pore size (nm)	EC (S/m)
0#	0.009	495	23.5	338.98
1#	0.015	511	16.5	213.22
2#	0.023	528	16.1	185.19
3#	0.036	548	14.5	182.48

Fig. 6 shows the particle size distribution curves of the doped aerogel powders (curves with different colors are the result of each sample tested for three times). Fig. 6 shows that the powder particle size from ~10 nm to 1 μm of micrometers range has a very wide distribution. It is proved that the powder mixture is composed of the many kinds of particles with sizes in nanoscale and micron meter scale. With the increase of magnetic doping, the size and distribution of particle size change slightly, which may be caused by the error in the experimental process. The

samples show a wide particle size distribution and are expected to interfere with electromagnetic signals at various bands.

In order to determine the existence form of doped Fe-compounds, the aerogels before and after doping were studied by XRD (Fig. 7). The results show that before doping, the aerogel only exhibits a wide peak around 13.25°, which is typical of amorphous carbon structure. Meanwhile, the XRD patterns of Fe-compounds reveal distinct peaks at 30.1° (220), 35.7° (311), 43.2° (400), 53.5° (422), 57.1° (511) and 62.7° (440), which is ascribed to the crystalline structure of Fe_3O_4. With the increase of the doping amount, the peak of Fe_3O_4 gradually becomes sharp, and the characteristic peak of carbon becomes weaker and narrower, indicating that there are already a large number of Fe_3O_4 nanoparticles in graphene carbon aerogels.

3.2 Electromagnetic interference performance of GN/CA/Fe_3O_4 aerogel powders

Fig. 8 shows the variation of the floating concentration of aerogels with different Fe_3O_4 doping amounts with time. The results in the Fig. 8 show that the concentration of the undoped aerogel sample 0#, the doped samples 1#, 2# and 3# show an obvious downward trend with the extension of the spreading time, and the decline of the powder tends to be obvious with the increase of the doping concentration. Among them, after 30 min of spraying, the concentration of 0# sample remains at 32%. The concentrations of Fe_3O_4 doped 1#, 2# and 3# samples were only 24%, 18% and 14% of the initial state, respectively after 30 min. This may be due to the increase of the density of the materials and the decrease of the floating time after doping with Fe_3O_4.

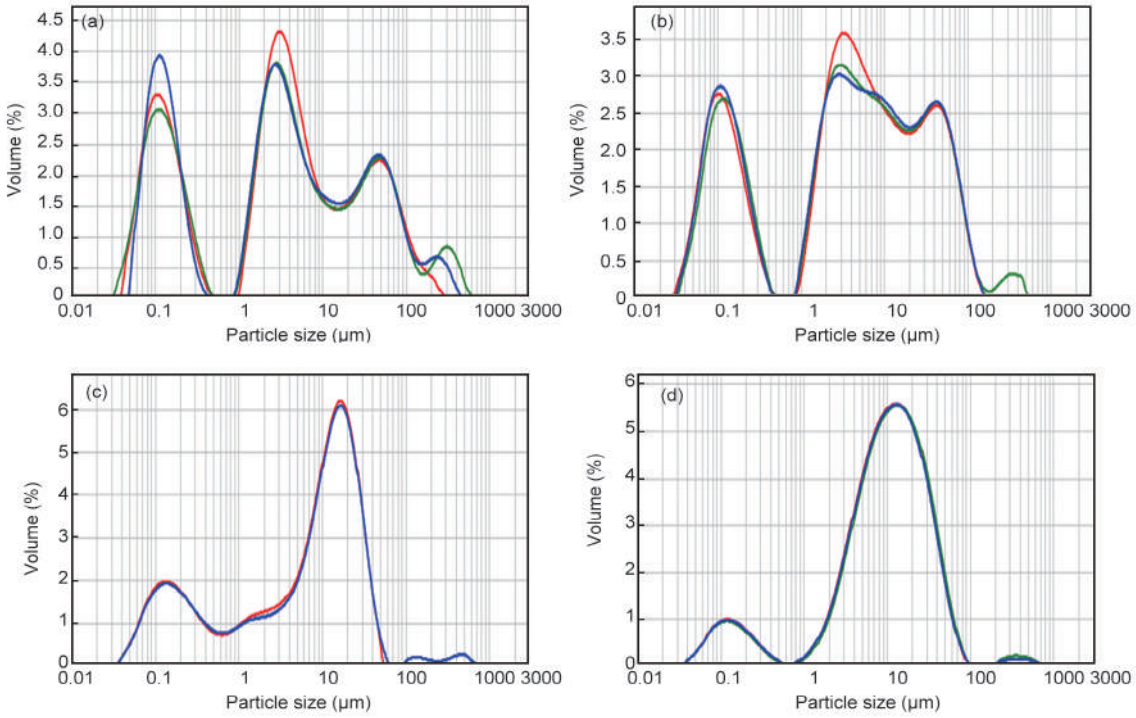

Fig. 6 Particle size distribution of the aerogel powder: (a) 0#, (b) 1#, (c) 2# and (d) 3#.

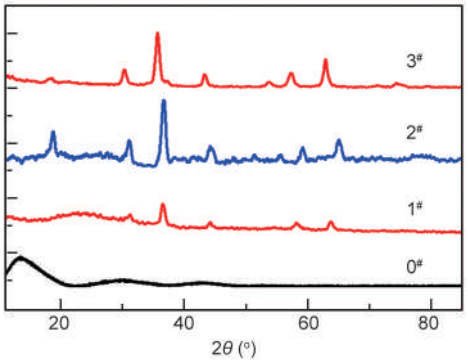

Fig. 7 XRD patterns of aerogel powders.

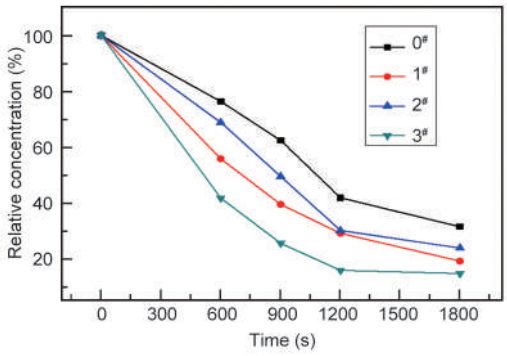

Fig. 8 The relative concentration change curves with time.

The electromagnetic interference performance of the aerogels for 3-5 μm infrared before and after doping is shown in Fig. 9 and Table 3 The results show that several kinds of aerogel powders have excellent interference performance, and the interference rate decreases with the increase of time. This is because with the extension of the time, the powder in the air gradually settles down, so that the actual concentration in the air decreases, the effective agent decreases. According to the change trend shown in the Fig. 9, the shielding ratios of undoped aerogel are 99.82% and 95.27% at the initial stage and 30 min after the distribution, respectively.

Compared with the undoped aerogel, the performance of 1# and 2# samples is improved by doping Fe_3O_4 nanoparticles, among which 2# sample with a high doping amount has the best performance. At the initial stage and after 30 min, the shielding ratios are 99.55% and 99.05% respectively, so the interference performance is significantly improved. In contrast, the shielding ratio of 3# sample with a high Fe_3O_4 doping is only 91.48% after 30 min. The interference performance is a comprehensive effect of density and electromagnetic performance. The interference performance of 3# sample is poor due to the fact that with a large amount of doping and excessive density, the interference performance decreases more after the rapid settlement of powder.

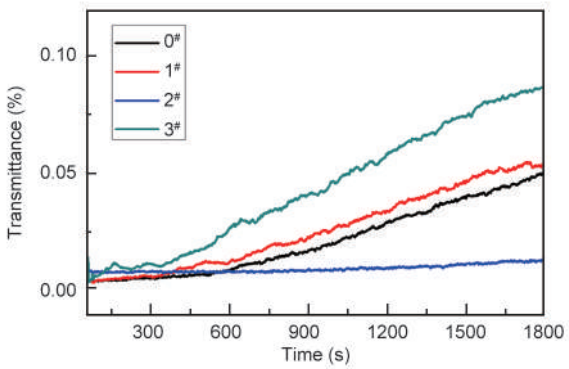

Fig. 9　The transmittance curves of aerogel powders in infrared light (3-5 μm).

Table 3　Shielding ratios of aerogel powders in infrared light (3-5 μm).

No.	300 s (%)	600 s (%)	1200 s (%)	1800 s (%)
0#	99.82 ± 2.0	99.59 ± 2.0	97.58 ± 2.0	95.27 ± 1.9
1#	99.79 ± 2.0	99.16 ± 2.0	96.98 ± 1.9	94.88 ± 1.9
2#	99.55 ± 2.0	99.61 ± 2.0	99.40 ± 2.0	99.05 ± 2.0
3#	99.20 ± 2.0	97.83 ± 2.0	94.67 ± 1.9	91.48 ± 1.8

The electromagnetic interference performance of aerogel for 8-12 μm infrared before and after doping is shown in Fig. 10 and Table 4. The results indicate that several kinds of aerogel powders show excellent interference performance, and the interference ratio decreases with the increase of scattering time, which is similar to that of 3-5 μm infrared. The shielding ratios of 0#, 1#, 2# and 3# samples are 97.5%, 99.16%, 99.35% and 99.28% after 5 min of interference, and 92.22%, 95.98%, 96.79% and 96.86% after 30 min of interference, respectively. It can be seen from the above results that, compared with the undoped sample, the shielding ratios of the material to the infrared is improved after doping the Fe_3O_4, and the interference performance of 2# sample is the best, which indicates that the magnetic oxide with a moderate doping amount is conducive to improve the electromagnetic interference performance of the material.

Table 4　Shielding ratios of aerogel powders in infrared light (8-12 μm).

No.	300s (%)	600s (%)	1200s (%)	1800s (%)
0#	97.5 ± 1.90	95.64 ± 1.90	93.34 ± 1.86	92.22 ± 1.84
1#	99.16 ± 1.98	98.51 ± 1.97	99.19 ± 1.98	95.98 ± 1.92
2#	99.35 ± 1.98	99.08 ± 1.98	99.78 ± 1.99	96.79 ± 1.93
3#	99.28 ± 1.98	98.92 ± 1.98	97.64 ± 1.95	96.86 ± 1.93

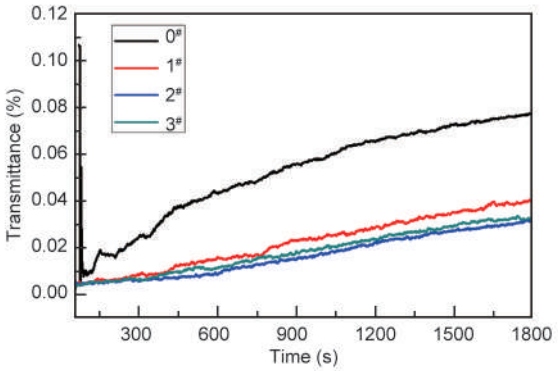

Fig. 10　The transmittance curves of aerogel powders in Infrared light (8-12 μm).

The visible light shielding performance of the doped material was tested, and the results are shown in Fig. 11. The results show that the interference performance of several aerogels is close to 99.5%. After 30 min, compared with 0# aerogel, the interference performance of the doped magnetic materials to visible light is improved to a certain extent, from 97.5% to 98.7%. The improvement effect of doping on interference performance is limited, which may be due to the fact that visible light of the material itself is almost completely covered, so the performance improvement effect after doping is not obvious.

The shielding performance of millimeter-wave is shown in Fig. 12 and Table 6. As can be seen from the curves in Fig. 11, after the initial spreading, the shielding ratios of 0#, 1#, 2# and 3# aerogel powders are 78.69%, 86.66%, 83.68% and 82.79%, respectively.

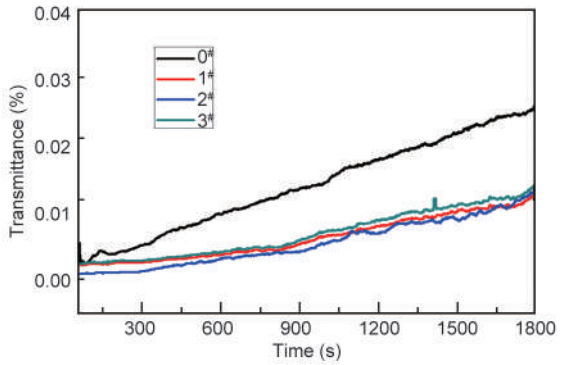

Fig. 11 The transmittance curves of aerogel powders in visible light.

Table 5 Shielding ratios of aerogel powders in Infrared light (8-12 μm).

No.	300 s (%)	600 s (%)	1200 s (%)	1800 s (%)
0#	99.52 ± 2.0	99.05 ± 1.98	98.3 ± 1.97	97.48 ± 1.95
1#	99.79 ± 2.0	99.67 ± 1.99	99.27 ± 1.98	98.8 ± 1.97
2#	99.90 ± 1.99	99.76 ± 1.99	99.34 ± 1.98	98.77 ± 1.97
3#	99.72 ± 1.99	99.62 ± 1.99	99.15 ± 1.98	98.67 ± 1.97

The MMW shielding performance shows similar trend with visible and infrared light, that is, compared with the undoped aerogel, the 2# has the better shielding performance. Compared with visible light and infrared, millimeter-wave shielding has a lower shielding ratio, which is due to the large size of microscopic particles acting on the millimeter-wave band, and the scale of this material system is still not enough to completely cover the millimeter band.

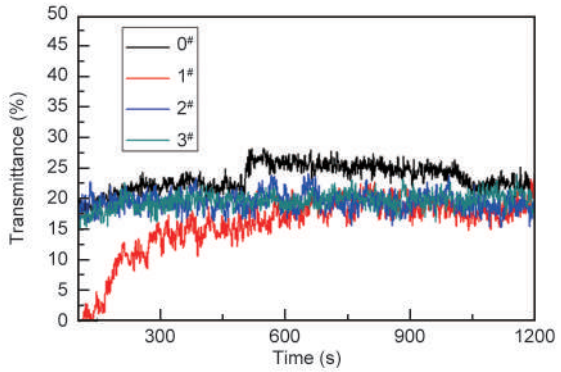

Fig. 12 The transmittance curves of aerogel powders in millimeter wavelength.

Table 6 Shielding ratios of aerogel powders in millimeter wavelength.

No.	300 s (%)	600 s (%)	1200 s (%)
0#	78.69 ± 1.57	74.05 ± 1.48	75.65 ± 1.57
1#	86.66 ± 1.73	82.62 ± 1.65	78.60 ± 1.57
2#	83.68 ± 1.61	83.15 ± 1.60	82.54 ± 1.61
3#	82.79 ± 1.61	81.75 ± 1.59	80.79 ± 1.61

3.3 Mechanism analysis

It can be seen from the above data that the doped aerogel powders have excellent shielding performance to visible light, infrared and millimeter wave, which is due to the following reasons (Fig. 13). First, a large number of free electrons exist on the surface because highly conductive graphene enhances the material's electrical conductivity, and some of the electromagnetic waves are immediately reflected. The remaining electromagnetic waves interact with the highly conductive lattice structures of graphene and carbon, creating a current that leads to ohm loss, which further weakens the energy of the waves [23]. Secondly, the graded micro-nano structure inside aerogel causes multistage reflection of electromagnetic waves after they enter the material, leading to internal loss and showing attenuation characteristics [24]. Thirdly, the doping of magnetic nanoparticles endows the aerogels with magnetic properties and can interact with electromagnetic waves to generate electromagnetic losses [25]. The combined action of the above forms makes the composite aerogel powders exhibit excellent multiband electromagnetic interference performance.

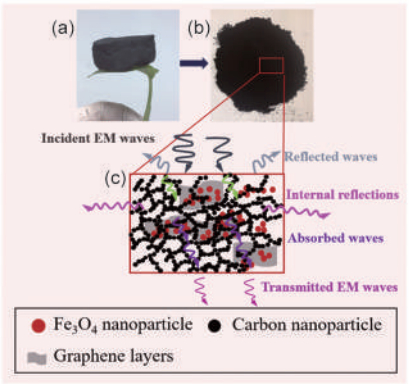

Fig. 13 Schematic illustration of mechanism for the composite aerogels. (a) Optical photograph of composite aerogels, (b) Optical photograph of composite aerogels powder and (c) diagram of the interaction between the aerogels and electromagnetic wave.

4 Conclusions

By controlling the gelation process and doping parameters, the ultralight magnetic graphene-carbon aerogel powders are prepared, and the ultralight magnetic graphene-carbon aerogel powder with the density of 0.015 g cm^{-3} and the specific surface area of 511 m^2 g^{-1} is realized.

Magnetic graphene co-doped carbon aerogel powders are prepared by controlling the composition and microstructure of the aerogels. The results show that the electromagnetic interference performance of the materials can be effectively improved by proper doping of magnetic nanoparticles. The improvement of the electromagnetic interference performance is the result of the compre-

hensive effect of the interference performance and the hysteresis effect. The optimization results show that the composite aerogel powder can achieve the effective shielding of three bands, the effective shielding time of infrared and visible light can be more than 30 min, and the visible light shielding ratio is greater than 98%. The shielding ratio of 3-5 μm infrared light is more than 99%, and the shielding ratio of 8-12 μm infrared light is more than 96%. The effective shielding time of millimeter wave can be above 30 min, and the shielding ratio is more than 82%.

References

[1] Chen H, Gao X B, Li T P, et al. Smoke screen jamming bombs development and key technology research abroad [J]. Aerodynamic Missile Journal, 2017, 10: 71-74.

[2] GAO Xiang-li, LIU Cui-xian, HAN Gao-yi, et al. Reduced graphene oxide hydrogels prepared in the presence of phenol for high-performance electrochemical capacitors [J]. New Carbon Materials, 2019, 34(5): 403-416.

[3] Yu N, Li J S, Wang X Z, et al. Simulation of jamming effect evaluation of IR smoke screen [J]. Transducer and Microsystem Technologies, 2012, 31: 23-25.

[4] Liu S T, Jiang N, Wang L T. Online evaluation method of shield jamming effects for ship-bome smoke screen [J]. Laser & Infrared, 2016, 46: 985-988.

[5] Lv T, Zhang E S, Yuan Y, et al. Preparation of large-size single layer mxene with low defect and electromagnetic shielding performance of MXene film [J]. Chem J Chinese Universities, 2019, 40: 2059-2066.

[6] Song W L, Guan X T, Fan L Z, et al. Magnetic and conductive graphene papers toward thin layers of effective electromagnetic shielding [J]. J. Mater. Chem. A, 2015, 3: 2097-2107.

[7] Song W L, Fan L Z, Cao M S, et al. Facile fabrication of ultrathin graphene papers for effective electromagnetic shielding [J]. J. Mater. Chem. C, 2014, 2: 5057-5064.

[8] Song W L, Guan X T, Fan L Z, et al. Tuning three-dimensional textures with graphene aerogels for ultra-light flexible graphene/texture composites of effective electromagnetic shielding [J]. Carbon, 2015, 93: 151-160.

[9] Liu X C, Zheng W P. Laser & infrared, study on extinction characteristic of nano-fe powders smoke screen to 1.06μm and 10.6μm Laser [J]. 2008, 38: 914-915.

[10] Du G P, Miu Y K, Zhang L. Study on attenuation performance of expansible graphite at 3mm wave [J]. Initiators & Pyrotechnics, 2005, 01: 14-16.

[11] Guan H. Research on anti-IR/MMW compound smoke composition technology (D). Nanjing university of science & technology, Nanjing, 2005.

[12] Yu S H. Infrareds and millimeter-wave composite interference materials [D]. Nanjing university of science & technology, Nanjing, 2009.

[13] Liu Z L, Wang X Y, Dong W J, et al. Composite interference performance of chopped carbon fiber clouds to millimeter wave and infrared [J]. Chinese Journal of Energetic Materials, 2016, 24: 1219-1224.

[14] Chen Hao, Gao X B, Xu X C, et al. Middle and far infrared interference properties of NT/graphene/carbon composites smoke screen [J]. Chinese Journal of Energetic Materials, 2019, 27: 249-254.

[15] Zhang E S, Lv T, Liu T. Preparation of graphene/carbon aerogel and its applied research in multi-frequency band electromagnetic interference [J]. Chem J Chinese Universities, 2019, 40: 567-575.

[16] Chen Z. Study on preparation and extinction properties of composite materials as combustion-type anti-infrared smoking agent (D). Nanjing university of science & technology, Nanjing, 2018.

[17] Li S F, Zha W K, Fang J J, et al. Extinction characteristic of graphene smoke to infrared and laser wave [J]. Infrared Technology, 2010, 32: 366-369.

[18] Wu Z S , Yang S B, Sun Y, et al. 3D nitrogen-doped graphene aerogel-supported Fe_3O_4 nanoparticles as efficient electro catalysts for the oxygen reduction reaction [J]. J Am Chem Soc, 2012, 134: 9082-9085.

[19] Wang H X, Song Z B, Yang N C, et al. Infrared extinction properties of randomly oriented columnar nano-graphite particles [J]. Advanced Materials Research, 2012, 602: 165-168.

[20] Du X, Liu H Y, Mai Y W. Ultrafast synthesis of multifunctional N-doped graphene foam in an ethanol flame [J]. ACS nano, 2016, 10: 453-462.

[21] Wan Y J, Zhu P L, Yu S H, et al. Anticorrosive, ultralight, and flexible carbon-wrapped metallic nanowire hybrid sponges for highly efficient electromagnetic interference shielding [J]. Small, 2018, 14: 1800534.

[22] Liu G, Ma W J, An X F, et al. Electromagnetic nterference shielding of single-wall carbon nanotube buckypaper /epoxy composites [J]. Carbon, 2012, 27: 101-104.

[23] Wen B, Cao M, Lu M, et al. Reduced graphene oxides: Lightweight and high-efficiency electromagnetic interference shielding at elevated temperatures [J]. Advanced Materials, 2014, 26: 3484-3489.

[24] Shahzad F, Alhabeb M, Hatter C B, et al. Electromagnetic interference shielding with 2D transition metal carbides (MXenes) [J]. Science, 2016, 353: 1137-1140.

[25] Pignard S, Vincent H, Flavin E, et al. Magnetic and electromagnetic properties of RuZn and RuCo substituted $BaFe_{12}O_{19}$ [J]. J Magn Magn Mater, 2003, 260: 437-446.